

# Edge Heat Transport in the Helical Divertor Configuration in LHD

S. Masuzaki, M. Kobayashi, T. Murase, T. Morisaki, N. Ohyabu, H. Yamada, A. Komori,  
and LHD Experiment Group

*National Institute for Fusion Science, 322-6 Oroshi-cho, Toki 509-5292, Japan*

e-mail : masuzaki@LHD.nifs.ac.jp

To realize energy supply by fusion reactor, divertor design is one of the most important issues. Understanding of mechanisms of determining heat flux and its profile on divertor plates is necessary for the design. In the Large Helical Device (LHD), the largest heliotron-type superconducting device, particle and heat deposition profiles on the divertor plates have been investigated by using Langmuir probes, thermocouples and an infrared camera. Unlike in the scrape-off layer in tokamaks with poloidal divertor configuration, field lines structure in the edge plasma region in LHD is complicated. There is a stochastic field lines layer outside the last closed flux surface (LCFS) in LHD, and residual islands are embedded in the layer. There are edge surface layers and laminar layers outside the stochastic field lines layer [1], and they connect to divertor plates. Field lines in the stochastic layer connect to divertor plates through the edge surface layer, and their connection length is longer than several hundred meters. On the other hand, connection length of field lines in the laminar layer is typically a few tens of meters, and these field lines do not approach LCFS. Therefore, long field lines are main channel of parallel transport of particle and energy from LCFS to divertor, and particles and energy come to laminar layer by cross-field transport in the edge plasma region. Consequently, particle and heat flux profiles on divertor plates are determined by field lines structure connecting divertor plates and balance of parallel and perpendicular transport. The footprint of field lines on divertor has three-dimensional structure in LHD, and thus, it is observed in experiment that particle and heat flux profiles on divertor plates differ according to location and operational magnetic configuration [2]. Operational conditions, such as density and heating power also affect the profiles in experiment, and it is considered to be caused by changing the balance of parallel and perpendicular transport. Three-dimensional plasma and neutral transport code, EMC3-EIRENE [3] has been applied to study edge transport in LHD [4], and comparisons of the edge electron temperature and particle flux profiles on divertor plates between experimental observations and numerical results have been conducted [5]. The results suggest that electron temperature affects edge diffusion properties larger than electron density [5].

In this study, we investigate the divertor particle and heat fluxes and their profiles in more detail. The inboard and top Langmuir probe arrays were utilized to measure the ion saturation current, that is, the particle flux, and electron density and temperature. Figure 1(a) and (b) show schematic views of the LHD poloidal cross-sections in which the Langmuir probe array embedded divertor plates were located. In board and top Langmuir probe arrays have 20 and 16 electrodes, respectively, and the spatial distance between electrodes is 6 mm. They are embedded along the edge of the divertor plates.

An infrared camera (AGEMA, observing wavelength: 3-5  $\mu\text{m}$ , time resolution: 66 ms/frame) was utilized to measure the heat flux profile on the divertor plate. The camera observed torus inboard side from outboard port as shown in Fig. 1(c). It cannot observe the divertor plate in which the inboard Langmuir probe array is embedded, but the corresponding divertor plate can be observed.

In order to analyze the transport in the edge region, the three dimensional edge transport code, EMC3-EIRENE, has been utilized. Because of technical difficulties, the three dimensional mesh for the code did not fully include the divertor legs. To analyze the particle and heat flux profiles on the divertor plates, one dimensional fluid equations were solved using the upstream plasma parameters with the assuming no radiation loss and perpendicular transport in the divertor legs. For the short field line length between the X-point and the divertor plates, these assumptions are reasonable. In this study, impurity transport and radiation were not taken into account.

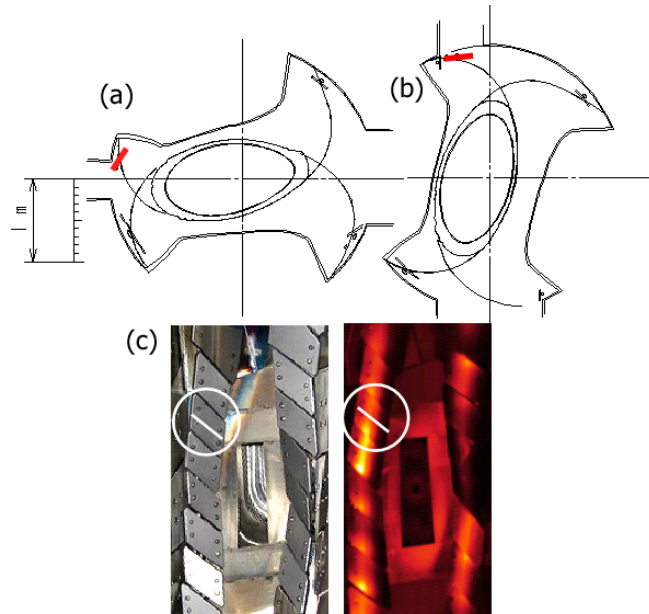


Fig.1. Poloidal cross-sections of LHD in which the (a) inboard and (b) top Langmuir probe array embedded divertor plates locate. In (a) and (b), the center of torus is on their left. The red lines in (a) and (b) show the position of the plates. (c) a field of view of the infrared camera. Right figure shows an infrared camera image during a discharge. White line on the divertor plate is the position of the inboard Langmuir probe array which is installed in other toroidal section.

Figures 2 show the heat flux profiles on a torus inboard divertor plate along the white line indicated in Fig. 1(c). Profiles of connection length of field lines are also plotted in each figure. These heat flux profiles were estimated from the temperature rises of the divertor plate at the just beginning of discharges using semi-infinite assumption with neglecting the heat diffusion in the plate. In the cases of  $R_{ax}=3.60$  and  $3.65$  m, there are several peaks of  $L_c$  over several hundred meter which come from the stochastic region. On the other hand, in the cases of  $R_{ax}=3.75$  and  $3.90$ m, the

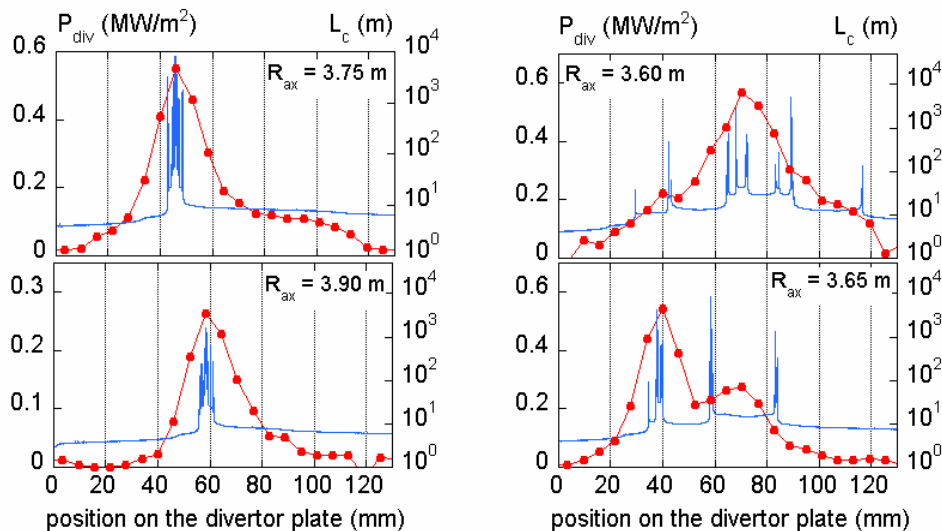


Fig. 2. Heat flux profiles for different operational magnetic configurations along the edge of the inboard divertor plate which is indicated in Fig. 1(c). “Rax” is the radial position of the magnetic axis. Profiles of connection length of field line are also depicted for each operational magnetic configuration.

long field lines connect to the divertor plate in relatively narrow region. Each heat flux profile reflects each  $L_c$  profile as particle flux case [2,5].

Heat flux during discharge is mainly estimated by using electron density and temperature measured by Langmuir probes with simple sheath model because the reconstruction of heat flux profile using infrared camera data has not been established up to now. A three dimensional finite-element method simulation code, ANSYS, has been applied to estimate the heat flux on the divertor plate. Heat flux estimated by using Langmuir probe data taking the incident angle of field lines to the divertor plate into account and infrared camera data are roughly agree with that estimated by ANSYS code.

We have frequently observed that the heat and particle flux profiles modified during discharge especially in the case of relatively inward shifted  $R_{ax}$  cases in which  $L_c$  profile has several peaks as shown in Figs. 2. Figure 3(a) shows a example of the modification of heat flux on an inboard-side divertor plate during discharge with  $R_{ax}=3.6m$ . Horizontal axis of Fig. 3(a) is same as in Figs. 2, but it is inverted. The profile at  $t=2.4-2.6s$  has its peak around the position of 70 mm as same as in the case of  $R_{ax}=3.6m$  in Figs. 2. The profile at  $t=1.1-1.3s$  has peaks at position of 55 and 35 mm. This modification of heat flux profile was also observed by infrared camera. Figures 3(b) and (c) show plasma parameters during the discharge, and the orange bars indicates the timing of the heat flux estimation in Fig.3(a). Figure 4 shows the heat flux profiles with different diffusion coefficients calculated by using EMC3-EIRENE code for  $R_{ax}=3.6m$  case. The heat flux profile in Fig. 3(a) at  $t=2.4-2.6s$  is similar to that in Fig. 4 with  $D=0.2m^2/s$  case. For the case of the heat flux profile in Fig. 3(a) at  $t=1.1-1.3s$ , calculation did not succeed to fully reproduce the profile. But the profile is relatively flat comparing with the other profile, and it seems that the diffusion is larger in  $t=1.1-1.3s$  case than the other. It should be noted that in spite of the about two times reduced heating power, the divertor heat flux at  $t=2.4-2.6s$  is larger than that at  $t=1.1-1.3s$ . It means the global heat deposition profile on the

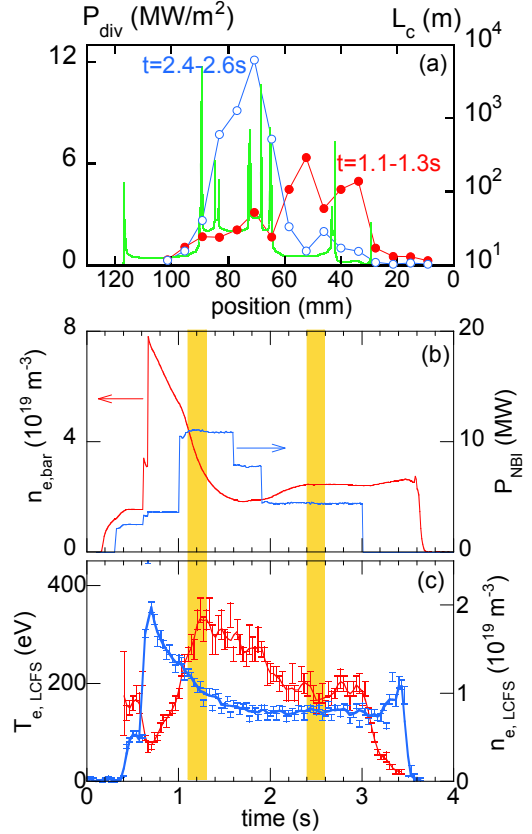


Fig. 3 (a) Heat flux profiles on the divertor plate at  $t=1.1-1.3s$  and  $t=2.4-2.6s$  in #65769 with  $R_{ax}=3.6m$ . Green line shows  $L_c$  profile. Horizontal axis is same as Figs. 2 but inverted. (b) Line averaged density and NB injection power, (c)  $T_e$  and  $n_e$  at LCFS in #65769.

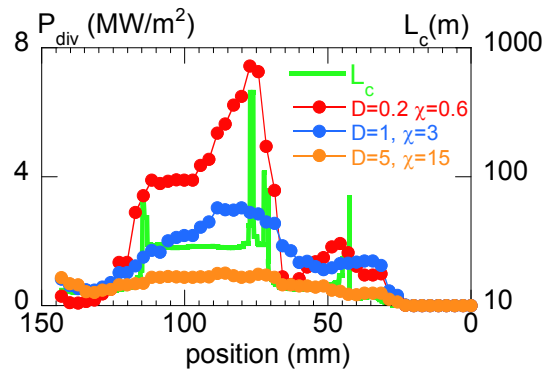


Fig. 4. Heat flux profiles at the same position as Figs.2 and 3(a) calculated by using EMC3-EIRENE code and  $L_c$  profile for the case of  $R_{ax}=3.6m$ . Three cases of diffusion coefficients, ( $D$  [m<sup>2</sup>/s],  $\chi$  [m<sup>2</sup>/s]), are calculated. The assumed power crossing the last closed flux surface (LCFS) is 10 MW, and electron density at LCFS is  $2 \times 10^{19}m^{-3}$ .

divertor modified. The calculation results in Fig. 4 show that the large diffusion causes the reduction of heat flux on this divertor plate. On the other hand, heat load increases on a top divertor plate as shown in Fig. 5. The difference between this plate and the inboard-side divertor plate shown in Figs. 3 and 4 is the dominant connection length of field lines. On the former plate, short field lines connect, and long field lines are dominant on the later plate. This result means that heat and particle transfer from long flux tube to short field lines region is enhanced. In experiment, heat flux profile on the top plate has not been measured, but increasing of the ratio of ion saturation current on the plate to that on the inboard-side plate has been observed.

What is the key parameter of the enhanced heat and particle transfer? Up to now, it looks be electron temperature. In the case of  $R_{ax}=3.6m$ , as described in the previous paragraph, electron temperature around LCFS at  $t=1.1-1.3s$  is about 300eV, and it is 200eV at  $t=2.4-2.6s$ . Density does not seem to be a critical parameter for the enhanced heat and particle transfer.

Figure 6 shows the peak heat flux estimated by using electron density and temperature measured by Langmuir probe on the inboard divertor plate as a function of  $P_{NBI}-P_{rad}$  for  $R_{ax}=3.75m$  configuration. In this configuration, heat flux profile on the plate is single peaked as shown in Fig. 2 and the insertion in Fig. 6. As indicated by blue and green lines, there are two trends. Electron temperature in blue trend is lower than 280 eV. On the other hand, it is higher than 320eV in the green trend. For the same heating power, heat flux on the divertor plate is relatively low in the green trend. That means heat transfer from “long” flux tube to laminar region is enhanced in the condition of green trend, and the condition seems to electron temperature. Figure 7 shows normalized heat flux ( $7I_{is}T_e \sin\alpha / (P_{NBI}-P_{rad})$ , where  $\alpha$  is the incident angle of field line on the divertor plate) on the inboard divertor plate versus ion-ion collision mean free path. All data is same as them in Fig. 6. This figure shows that the normalized heat flux decreases with increasing collision mean free path. This is contrary to simple consideration that the diffusion is enhanced by collision. The mechanism of the enhanced heat and particle transfer from long flux tube to short field lines region has not been understood.

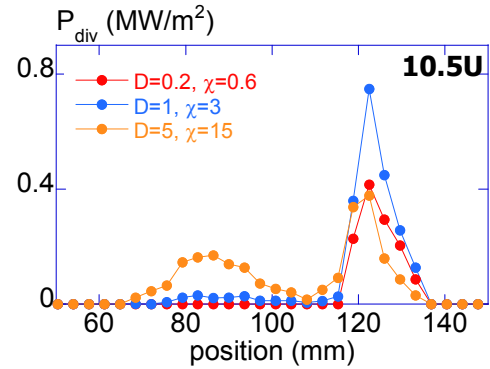


Fig. 5. Calculated heat flux profiles on a top divertor plate with different cross-field transport coefficients. Unit of the coefficients is  $m^2/s$ .

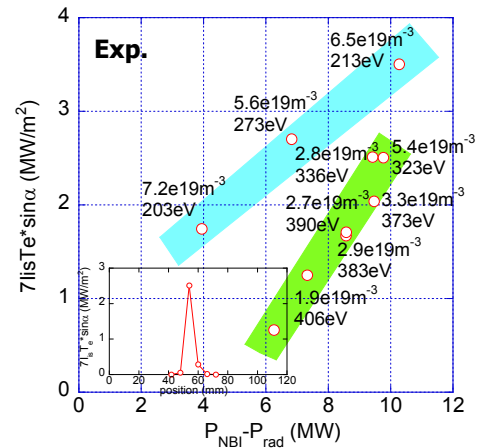


Fig. 6. Normalized heat flux on the inboard divertor plate vs. plasma heating power. The insertion is the heat flux profile on the plate. Electron density and temperature around LCFS are indicated for each data point.

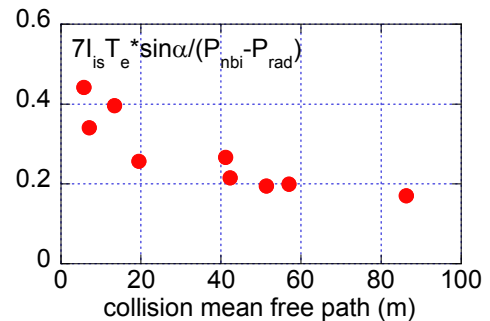


Fig. 7. Normalized heat flux on the torus inboard divertor plate vs. collision mean free path around the last closed flux surface in  $R_{ax}=3.75m$  configuration.

- [1] N. Ohyabu et al., Nucl. Fusion **34** (1994) 387.
- [2] S. Masuzaki et al., Fusion Sci. Tech. **50** (2006) 361.
- [3] Y. Feng et al., Nucl. Fusion **46** (2006) 807.
- [4] M. Kobayashi et al., J. Nucl. Mater. **363-365** (2007) 294.
- [5] S. Masuzaki et al., J. Nucl. Mater., **390-391** (2009) 286.